LBL-26900

Lawrence Berkeley Laboratory
UNIVERSITY OF CALIFORNIA

Accelerator & Fusion
Research Division

Presented at the Workshop on Highly Charged Ions: New Physics and Advanced Techniques, Lawrence Berkeley Laboratory, Berkeley, CA, March 13–15, 1989, and to be published in Nuclear Instruments and Methods in Physics Research B

Multiple-Electron Processes in Fast Ion-Atom Collisions

A.S. Schlachter

March 1989

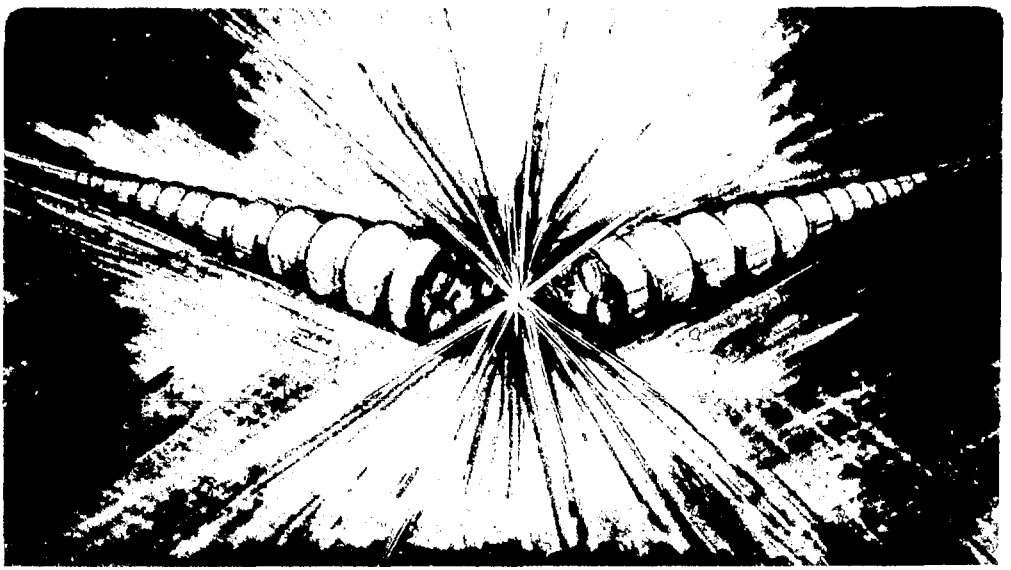

Prepared for the U.S. Department of Energy under Contract Number DE-AC03-76SF00098.

LBL--26900

DE89 012982

Multiple-Electron Processes in Fast Ion-Atom Collisions

A.S. Schlachter

Accelerator and Fusion Research Division
Lawrence Berkeley Laboratory
1 Cyclotron Road
Berkeley, California 94720

Paper presented at the Workshop on Highly Charged Ions: New Physics and Advanced Techniques, Lawrence Berkeley Laboratory, March 13-15, 1989.

To be published in Nuclear Instruments and Methods.

Version 1.5 13 April 89

Multiple-Electron Processes in Fast Ion-Atom Collisions*

A.S. Schlachter
Lawrence Berkeley Laboratory
Berkeley, CA 94720

Research in atomic physics at the Lawrence Berkeley Laboratory Super-HILAC and Bevalac accelerators on multiple-electron processes in fast ion-atom collisions is described. Experiments have studied various aspects of the charge-transfer, ionization, and excitation processes. Examples of processes in which electron correlation plays a role are resonant transfer and excitation and Auger-electron emission. Processes in which electron behavior can generally be described as uncorrelated include ionization and charge transfer in high-energy ion-atom collisions. A variety of experiments and results for energies from 1 MeV/u to 420 MeV/u are presented.

* This work was supported the Director, Office of Energy Research, Office of Fusion Energy, U.S. DOE under Contract No. DE-AC03-76SF00098.

I. Introduction

Charge transfer, ionization, and excitation are fundamental processes in fast ion-atom collisions. Each of these processes can occur alone in a single collision, or more than one process can take place in a single collision. When more than one electron is involved, electron correlation, due to an electron-electron interaction, can be important, as in resonant transfer and excitation (RTE) or in Auger-electron emission. When electron correlation is not important, the process can be described by an independent electron model, as is generally the case, for high-energy ion-atom collisions, in continuum-electron emission, multiple-electron capture in close collisions, and recoil-ion production.

All of these processes have been studied at the Lawrence Berkeley Laboratory, using fast ion beams from the SuperHILAC and Bevalac accelerators. The topics discussed in this paper are charge transfer, recoil-ion production, continuum-electron production, multiple-electron capture in close collisions. the radiative Auger effect, and RTE. Discussion of RTE includes observation by particle-x-ray coincidence for excitation of the K and L shells of the projectile, and by non-coincident electron capture. This paper mentions the work of over 40 atomic physicists from LBL and many other institutions who have worked at the Super-HILAC and Bevalac accelerators in recent years; the references contain a more complete discussion of apparatus, methods, and results.

2. Charge Transfer

Cross sections for electron capture and electron loss have been measured for a wide variety of multiply charged ions for energies from 0.3 to 8.5 MeV/u at the SuperHILAC, and energy and charge-state dependences have been determined [1-3]. An example is shown in Figs. 1 and 2, in which the cross sections for electron capture and electron loss are shown as a function of energy for $_{23}V^{20+}$ on He and as a function of projectile charge state for 8.55 MeV/u vanadium ions in He. Figure 1 shows energy dependence of electron-capture and electron-loss cross sections for V^{20+} in He. The figure shows the broad maximum expected for electron loss near the maximum of the cross section; it also shows the steep decrease in electron capture with increasing projectile energy. The electron-capture data shown have an energy dependence of approximately $E^{-4.2}$ for the higher energies. Born-approximation calculations predict an electron-capture energy dependence which should reach a limit of $E^{-5.5}$ (second Born) or E^{-6} (first Born) at asymptotically high energies. Figure 2 shows the charge-state dependence of electron-capture and electron-loss cross sections for 8.55 MeV/u $_{23}V^{q+}$ in He. Clearly seen is the shell effect in electron loss: the cross section decreases by a large factor for removal of a projectile K electron. This discontinuity for electron loss between q = 20 and q = 21 marks the boundary between the vanadium L and K shells. Electrons in the K shell of vanadium are bound by about 6.5 keV, while those in the L shell are bound by

less than 1.6 keV. The L-shell electron-loss cross section is found to scale as q^{-12}, while the K-shell electron-loss cross section scales as q^{-14}. The electron-capture cross sections scale as $q^{-3.8}$, midway between the OBK scaling for intermediate velocities of q^3 and the second-Born-approximation high-energy prediction of q^5. Early charge-transfer results have been summarized [4] and a scaling rule for electron capture has been determined [5]. This scaling rule is useful for predicting the magnitude of as-yet unmeasured cross sections. Projectile electron loss and excitation have also been reported [6]. Similar measurements at much higher energies have been made by Gould and co-workers [7] at the Bevalac.

3. Ionization: Recoil-Ion Production

Multiple ionization of rare-gas atoms by highly charged uranium ions has been studied at the Bevalac [8,9]. Two experiments have been performed to measure the recoil-ion charge-state distribution by a coincidence time-of-flight method. Cross sections for multiple ionization of Ne, Ar, Kr, and I atoms by 420 MeV/u U^{n+} (n~91) were measured; recoil-ion charge states up to approximately 0.5 times the target atomic number were identified. Figure 3 shows the measured ionization cross sections as a function of recoil-ion charge state. The cross sections are large, e.g., greater than 10^{-18} cm^2 for producing Kr recoil ions in charge states around 20+. Error bars on q arise from uncertainty in the time calibration. Results are shown in Fig. 3. Similar measurements were made in Ne, Ar, and Kr targets for 120 MeV/u U^{90+} projectiles, shown in Fig. 4. These measurements have allowed comparison of ionization cross sections for uranium-ion impact on rare-gas targets over the energy range 1.4 to 420 MeV/n. The data are nicely described by n-body CTMC calculations. The calculations indicate the importance of accounting for Auger events in describing the multiple-ionization process.

4. Continuum-electron production

Electron-emission cross sections differential in angle and electron energy have been measured for 6 MeV/u U^{38+} and Th^{38+} on He and Ar targets [10]. The apparatus is shown in Fig. 5. Figure 6 shows doubly differential cross sections for 6-MeV/u U^{38+} in Ar for a forward angle (30°) and a background angle (150°), along with a Plane Wave Approximation (PWBA) calculation. The electron emission shows an enhancement at forward angles and a decrease at backward angles relative to scaled cross sections based on the Born approximation, arising from the two-center nature of the collision. Also seen in the figure is a feature due to Ar L-Auger-electron emission. Results are also compared with CTMC calculations in Ref. 10. Future experiments are planned, in which electron emission in coincidence with projectile charge transfer will be studied.

5. Resonant transfer and excitation (RTE)

Resonant transfer and excitation (RTE) is a well-established example of electron correlation in ion-atom collisions. Electron correlation arises from the electron-electron interaction, and is observed only in certain cases in atomic physics, e.g., Auger-electron emission. In fact, RTE, in which one electron is captured from a target atom by a highly charged projectile ion while another electron in the projectile is simultaneously excited, is the ion-atom analogue of dielectronic recombination, which is the formation of an excited intermediate state via an inverse Auger transition. RTE is resonant when the projectile velocity is such that the energy of a target electron in the rest frame of the projectile is equal to one of the Auger electron energies. Many intermediate excited states are possible, each one corresponding to an allowed Auger transition. The intermediate excited state produced in the RTE process can stabilize by x-ray emission, in which case its signature is detection of an x-ray in coincidence with a projectile which has captured an electron. The intermediate excited state can also stabilize by Auger-electron emission.

Resonant transfer and excitation involving excitation of a K-shell electron has been measured by x-ray-particle coincidence techniques [11-12]. An example is shown in Fig. 7, for Ca^{q+} ions (q=10-19) in H_2, i.e., in charge states from neon-like to hydrogen-like. The structure with energy is explained by two groups of intermediate excited states. These measurements have been extended to excitation of an L-shell electron for heavier projectiles [13]; Fig. 8 shows L-shell RTE measurements for Nb^{31+} in H_2. Cross sections for L-shell RTE are found to be about a factor of ten larger than those found for RTE involving the K shell, and to constitute as much as half of the total $L_{\alpha\beta}$ x-ray production. Overall agreement with theory is reasonable.

The first observation of non-monotonic behavior in the energy dependence of an electron-capture cross section for a high-energy ion-atom collision was reported in Ref. 14. Structure in the energy dependence of high-energy electron capture was found to be attributable to RTE, as measured in a singles (non-coincident) experiment [14]. This result is shown in Fig. 9, for $Ca^{17+} + H_2$. For comparison, the same cross section for Ca^{17+} + He, in which RTE is smaller, is shown in Fig. 10. The ratio of the cross section for RTE relative to that for normal electron capture is expected to be greater at higher projectile velocities. Recent measurements [15] have looked for RTE in a single-electron capture measurement for U^{89+} on C at energies from 130-160 MeV/u at the LBL Bevalac accelerator. Results are presently being analyzed.

6. Multiple electron capture in close collisions.

Close collisions between an energetic projectile ion and a target atom can be selected by detection of a projectile or target K x-ray: the K x ray is evidence that a K-shell vacancy was produced in a collision at small impact parameter. If one selects a projectile with an empty or nearly empty L shell and having a velocity similar to that of electrons in the target L shell, as is the case for 47-MeV Ca^{17+} in an Ar target [16,17], the cross sections for capturing several electrons are found to exceed that for the capture of only one electron. This result is shown in Fig.11. The corresponding electron-capture charge-state distribution can be fit with a binomial distribution, as is shown in Fig. 12, giving an electron-capture probability of nearly 0.5. The agreement of the data with a binomial distribution is consistent with independent electron capture, and suggests an absence of electron correlation in the multiple-electron-capture process. Total electron-capture cross sections, in which close collisions are not selected, are found to be much larger than the x-ray coincidence cross sections, and to decrease monotonically with increasing number of electrons captured (Fig. 13).

Multiple-electron capture in close collisions of highly charged Ca ions has been studied for a variety of conditions. Increasing the Ca-ion velocity is found to lead to a decrease in the electron-capture probability, as would be expected: the projectile is fast relative to the velocity of electrons in the L shell of the target atom. Another experiment [18] was to vary the number of vacancies in the L shell of the Ca projectile from none (neon-like Ca^{10+}) to seven (lithium-like Ca^{17+}). The electron-capture probability is found to be a linear function of the number of initial vacancies in the projectile L shell. This suggests direct transfer of electrons from the L and M shells of the target to the L shell of the projectile.

Experimental K-K vacancy-sharing probabilities can be calculated from the observed cross sections for electron capture in coincidence with a Ca or Ar K x-ray, corrected by neutral-atom fluorescence yields. For capture of up to 4 electrons, this vacancy-sharing probability is found to be independent of the number of electrons captured (Fig. 14), and is in good agreement with the theoretical value calculated from the relation given by Meyerhof and obtained using neutral-atom K binding energies This independence is evidence that the mechanism producing the K vacancies can be considered as separate from the L-shell electron-capture process.

7. Radiative Auger emission

An unusual decay mode for an ion with an inner-shell vacancy is the radiative Auger effect (RAE), in which filling of an inner-shell vacancy is accompanied by the simultaneous emission of a photon and an electron. Measurements have been made [20] of projectile x-ray spectra coincident with single-electron loss in collisions of 3.5-9.0-MeV/u V^{q+}(q=19,20,21) ions with He targets under single-collision conditions. Non-monoenergetic x-rays observed in the coincidence spectra for V^{20+} (lithium-like) projectiles are attributed to RAE. Results are shown in Fig. 15. The intensity of RAE photons relative to the characteristic K x-ray yield is more than an order of magnitude larger than expected from theoretical calculations and from earlier measurements for atomic targets. However, the calculations and previous experiments involved ions with relatively few electron vacancies. The large relative enhancement of the RAE rate for lithium-like V^{20+} is most probably due to the small number of electrons on these ions.

REFERENCES

1. W.G. Graham, K.H. Berkner, R.V. Pyle, A.S. Schlachter, J.W. Stearns, and J.A. Tanis, "Charge-transfer cross sections for multiply charged ions colliding with gaseous targets at energies from 310 keV/amu to 8.5 MeV/amu," *Phys. Rev.* A 30, 722 (1984).

2. E.C. Montenegro, Xiang-Yuan Xu, R. Anholt, K. Danzmann, W.E. Meyerhof, A. S. Schlachter, B. S. Rude, and R. J. McDonald, "Intermediate-velocity atomic collisions. III. Electron capture in 8.6-MeV/amu Ca ions," *Phys. Rev.* A 38, 1848 (1988).

3. W.G. Graham, K.H. Berkner, E.M. Bernstein, M. Clark, R.H. McFarland, T.J. Morgan, A.S. Schlachter, J.W. Stearns, M.P. Stockli, and J.A. Tanis, "Charge-state dependence of single-electron-capture and -loss cross sections for highly stripped V ions in He at 8.55 MeV amu^{-1}," *J. Phys.* B 18, 2503 (1985); A. S. Schlachter, K. H. Berkner, J. W. Stearns, W. G. Graham, E. M. Bernstein, M. W. Clark, J. A. Tanis, H. Schmidt-Böcking, S. Kelbch, J. Ullrich, S. Hagmann, P. Richard, M. P. Stockli, and A. Müller, "Ionization and charge transfer in high-energy ion-atom collisions," *Nucl. Instrum. Methods* B 24/25, 219 (1987).

4. A.S. Schlachter."Charge-changing collisions," *Proceedings of the Tenth International Conference on Cyclotrons and Their Applications, April 30-May 3, 1984.*

5. A.S. Schlachter, J.W. Stearns, W.G. Graham, K.H. Berkner, R.V. Pyle, and J.A. Tanis, "Electron capture for fast highly charged ions in gas targets: an empirical scaling rule," *Phys. Rev.* A 27, 3372 (1983).

6. Xiang-Yuan Xu, E.C. Montenegro, R. Anholt, K. Danzmann, W.E. Meyerhof, A. S. Schlachter, B. S. Rude, and R. J. McDonald, "Intermediate-velocity atomic collisions. II. K-shell ionization and excitation in 8.6-MeV/amu Ca ions," *Phys. Rev.* A 38, 1848 (1988).

7. Harvey Gould, Douglas Greiner, Peter Lindstrom, T.J.M. Symons, and Henry Crawford, "Electron capture by U^{91+} and U^{92+} and ionization of U^{90+} and U^{91+}," *Phys. Rev. Lett.* 52, 180 (1984); R. Anholt, W.E. Meyerhof, X.Y. Xu, H. Gould, B. Feinberg, R.J. McDonald, H.E. Wegner, and P. Thieberger, *Phys. Rev.* A 36, 1586 (1987).

8. S. Kelbch, J. Ullrich, W. Rauch, H. Schmidt-Böcking, M. Horbatsch, R.M. Dreizler, S. Hagmann, R. Anholt, A.S. Schlachter, A. Müller, P. Richard, Ch. Stoller, C.L. Cocke, R. Mann, W. E. Meyerhof, and J.D. Rasmussen, "Multiple ionisation of Ne, Ar, Kr and I by nearly relativistic U ions," *J. Phys.* B 19, L47 (1986).

9. H. Berg, R. Dörner, C. Kelbch, S. Kelbch, J. Ullrich, S. Hagmann, P. Richard, H. Schmidt-Böcking, A.S. Schlachter, M. Prior, H. J. Crawford, J. M. Engelage, I. Flores, D. H. Loyd, J. Pedersen, and R. E. Olson, "Multiple ionisation of rare gases by high-energy uranium ions," *J. Phys.* B 21, 3929 (1988).

10. D. Schneider, A.S. Schlachter, R.E. Olson, W. G. Graham, J. R. Mowat, R. D. DuBois, D. DeWitt, D. H. Loyd, V. Montemayor, G. Schiwietz, "Observation of strong continuum-continuum couplings in the direct ionization of Ar and He atoms by 6-MeV/u U^{38+} and Th^{38+} projectiles," *Phys. Rev.* A (in press).

11. J.A. Tanis and E.M. Bernstein, W.G. Graham, M. P. Stockli, M. Clark, R. H. McFarland, T.J. Morgan, K. H. Berkner, A.S. Schlachter, and J.W. Stearns, "Resonant electron transfer and excitation in two-, three-, and four-electron $_{20}Ca^{q+}$ and $_{23}V^{q+}$ ions colliding with Helium," *Phys. Rev. Lett.* 53, 2551 (1984).

12. J.A. Tanis, E.M. Bernstein, M.W. Clark, W.G. Graham, R.H. McFarland, T.J. Morgan, J. R. Mowat, D. W. Mueller, A. Müller, M. P. Stockli, K. H. Berkner, P. Gohil, R. J. McDonald, A. S. Schlachter, and J.W. Stearns, "Resonant transfer and excitation: Dependence on projectile charge state and target-electron momentum distribution," *Phys. Rev.* A 34, 2543 (1986).

13. E. M. Bernstein, M. W. Clark, J. A. Tanis, K. H. Berkner, R. J. McDonald, A. S. Schlachter, J. W. Stearns, W. G. Graham, R. H. McFarland, T. J. Morgan, J. R. Mowat, D. W. Mueller, and M. P. Stockli, "Resonant electron transfer and L-shell excitation for $_{41}Nb^{31+}$ and $_{57}La^{40+}$ ions," *J. Phys.* B 20, L505 (1987).

14. W. G. Graham, E. M. Bernstein, M. W. Clark, J. A. Tanis, K. H. Berkner, P. Gohil, R. J. McDonald, A. S. Schlachter, J. W. Stearns, R. H. McFarland, T. J. Morgan, and A. Müller, "Structure in the energy dependence of high-energy electron-capture cross sections," *Phys. Rev.* A 33, 3591 (1986).

15. W.G. Graham, K.H. Berkner, E.M. Bernstein, M.W. Clark, B. Feinberg, R.J. McDonald, P.M. Mokler, T.J. Morgan, W. Rathbun, A.S. Schlachter, J.A. Tanis, H. Crawford, I. Flores, and L. Greiner, "The Search for RTE in 30-38 GeV collisions of U^{89+} with carbon foils," paper submitted to ICPEAC, 1989.

16. A. S. Schlachter, E. M. Bernstein, M. W. Clark, R. D. DuBois, W. G. Graham, R. H. McFarland, T. J. Morgan, D. W. Mueller, K. R. Stalder, J. W. Stearns, M. P. Stockli, and J. A. Tanis, "Multiple-electron capture in close nearly symmetric ion-atom collisions," *J. Phys.* B 21, L291 (1988).

17. A. S. Schlachter, J. W. Stearns, K. H. Berkner, E. M. Bernstein, M. W. Clark, R. D. DuBois, W. G. Graham, T. J. Morgan, D. W. Mueller, M. P. Stockli, J.

A. Tanis, and W. T. Woodland, "Close encounters of the multiple-capture kind: Ca ions in Ar," *Nucl. Instrum. Methods* (in press).

18. A. S. Schlachter, K. H. Berkner, E. M. Bernstein, M. W. Clark, R. D. DuBois, W. G. Graham, T. J. Morgan, D. W. Mueller, J. W. Stearns, M. P. Stockli, J. A. Tanis, and W. T. Woodland, "Multiple-electron capture for 47-MeV calcium ions in argon: Projectile charge-state dependence," paper submitted to ICPEAC, 1989.

19. W. E. Meyerhof, *Phys. Rev. Lett.* 31, 1341 (1973).

20. E. M. Bernstein, M. W. Clark, K. H. Berkner, W. G. Graham, R. H. McFarland, T. J. Morgan, A. S. Schlachter, J. W. Stearns, M. P. Stockli, and J. A. Tanis, "Enhancement of radiative Auger emission in lithium-like $_{23}V^{20+}$ ions," *J. Phys.* B 21, L509 (1988).

FIGURE CAPTIONS

Fig. 1 The energy dependence of the single-electron-loss cross sections, $\sigma_{q,q+1}$ (□), and single-electron-capture cross sections, $\sigma_{q,q-1}$(○), for V^{20+} ions incident on He.

Fig. 2 Single-electron-loss cross sections, $\sigma_{q,q+1}$ (■), and single-electron-capture cross sections, $\sigma_{q,q-1}$(●), for 8.55 MeV/u V^{q+} ions incident on He.

Fig. 3 Measured cross sections σ(q) for the production of recoil ions by 420 MeV/u U^{n+} impact (n≃91) verses recoil-ion charge state, q. The targets were: Δ, I; □, Kr; ○, Ar; and ◊, Ne.

Fig. 4 Comparison of measured recoil-ion-production cross sections σ(q) with nCTMC calculations: ○, experiment; –, calculations with autoionization included; ---, calculations with autoionization not included.

Fig. 5 Experimental arrangement for electron spectroscopy at the LBL SuperHILAC accelerator.

Fig. 6 Doubly differential cross section for electron emission in collisions of 6-MeV/u U^{38+} in Ar. The dashed line shows the Plane-Wave Born Approximation calculation. Results are shown at forward (30°) and backward (150°) angles.

Fig. 7 Cross sections for projectile K x rays coincident with single-electron capture, $\sigma_{K\alpha\beta}^{q-1}$, for collisions of Ca^{q+} ions with H_2 (q=10, 11, 12, 16, 17, 18, and 19). The solid curves are drawn to guide the eye. Note the scale change for the $Ca^{10,11,12+}$ data.

Fig. 8 Cross sections for the total projectile L-x-ray production, $\sigma_{L\alpha\beta}$, and for the production of L x-rays coincident with single-electron capture, $\sigma_{K\alpha\beta}^{q-1}$, for collisions of neon-like Nb^{31+} with H_2. The vertical bars along the energy axis give the theoretical positions and relative intensities of the strongest

Auger transitions involving 2p excitations. The intermediate excited-state configurations of the two active electrons involved in the RTE process are indicated. The solid line is the predicted RTE cross section, σ_{RTE}, based on the theoretical DR cross section calculations of Hahn et al. (1987).

Fig. 9 Cross sections for Ca^{17+} in H_2. Filled circles are the cross sections for single-electron capture, $\sigma_{q,q-1}$; open circles are the cross sections for single-electron capture coincident with K-x-ray emission, $\sigma_{K\alpha\beta}^{q-1}$ The solid line is drawn to guide the eye. The dashed line shows an $E^{-4.2}$ energy dependence normalized to the point at 150 MeV.

Fig. 10 Single-electron-capture cross section $\sigma_{q,q-1}$ for Ca^{17+} in He. The line is a fit to the function $\sigma_{q,q-1}=\sigma_0 E^{-4.2}$, passing through the point at 141 MeV.

Fig. 11 Cross sections for electron capture in coincidence with Ar or Ca K x-ray for 47-MeV Ca^{17+} in Ar, as a function of the number of L- and M-shell electrons captured. The upper scale shows the projectile final charge state for coincidence with a Ca K x-rays. The Ar K x-ray coincidence data have been shifted one charge state to the left to account for the promotion of an Ar K electron to the Ca L shell for the case of emission of an Ar K x-ray.

Fig. 12 Relative electron-capture probabilities for 47-MeV Ca^{17+} in Ar as a function of the number of L- and M-shell electrons transferred, for coincidence with a Ca K or Ar K x-ray. The distribution for coincidence with an Ar K X-ray has been shifted to the left by one charge state. Solid bars show the experimental results; shaded bars show the binomial distribution for an electron-capture probability of 0.47 (assuming seven electrons can be captured).

Fig. 13 Electron-capture cross sections for 47-MeV Ca^{17+} in Ar, as a function of the final charge state of the projectile and of the number of electrons captured. Lower curve shows electron capture for a close collision, i.e., coincident with an Ar or Ca K x-ray; the upper curve shows total (non-coincident) electron capture.

Fig. 14 K-K vacancy-sharing probabilities as a function of the number of L- and M-shell electrons captured, for close collisions of 47-MeV Ca^{17+} in Ar. Experimental data and the theoretical value [19] are shown.

Fig. 15 Energy dependences of the cross sections for projectile K x-ray emission with no charge change, $\sigma^{20+}_{K\alpha\beta}$ (●) (left scale) and for RAE x-rays, σ_{RAE}(■) (right scale) in collisions of V^{20+} with He. The solid curve drawn through the $\sigma^{20+}_{K\alpha\beta}$ data points is to guide the eye. The dashed curve was calculated by taking 7.2% of the full curve (note that the left and right scales are different).

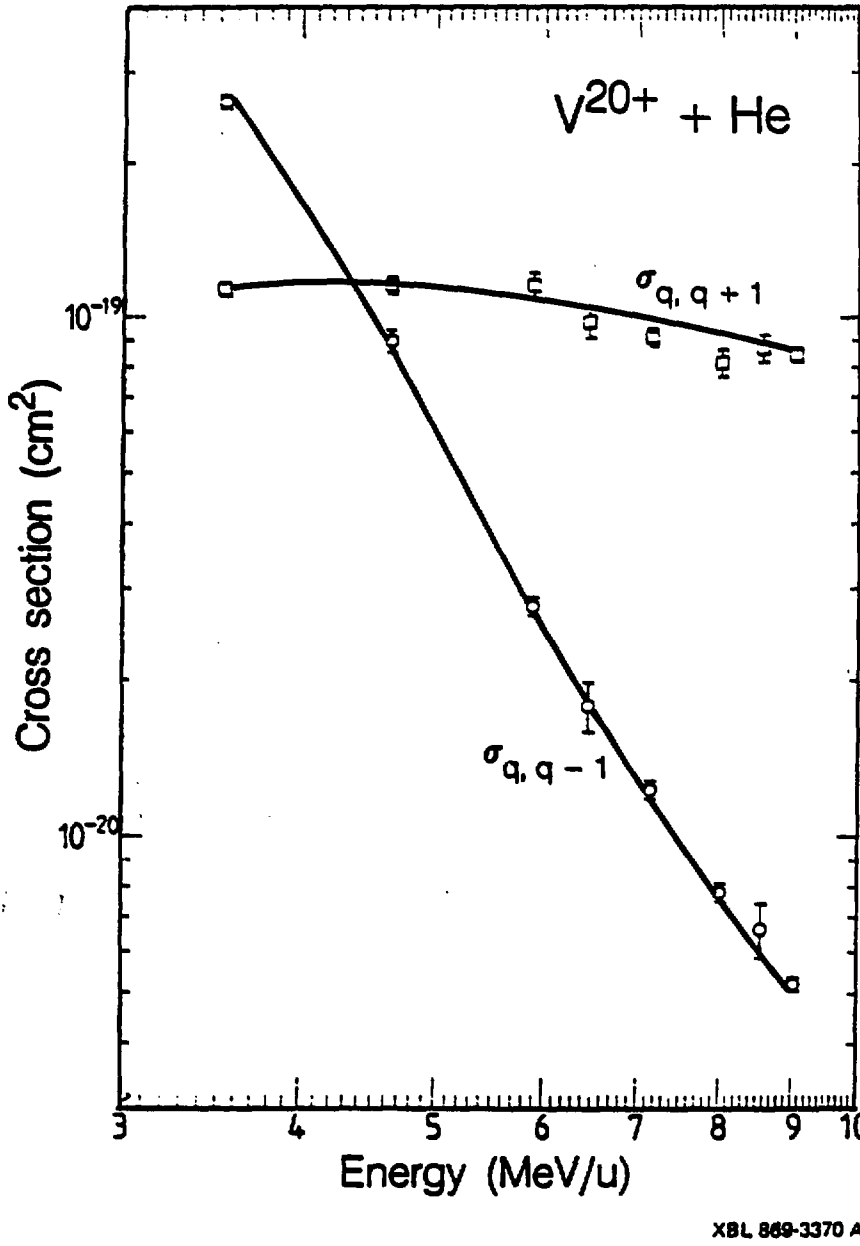
V^{20+} + He
$\sigma_{q,\,q+1}$
$\sigma_{q,\,q-1}$
10^{-19}
10^{-20}
Cross section (cm^2)
3
4
5
6
7
8
9
10
Energy (MeV/u)
XBL 869-3370 A

Figure 1.

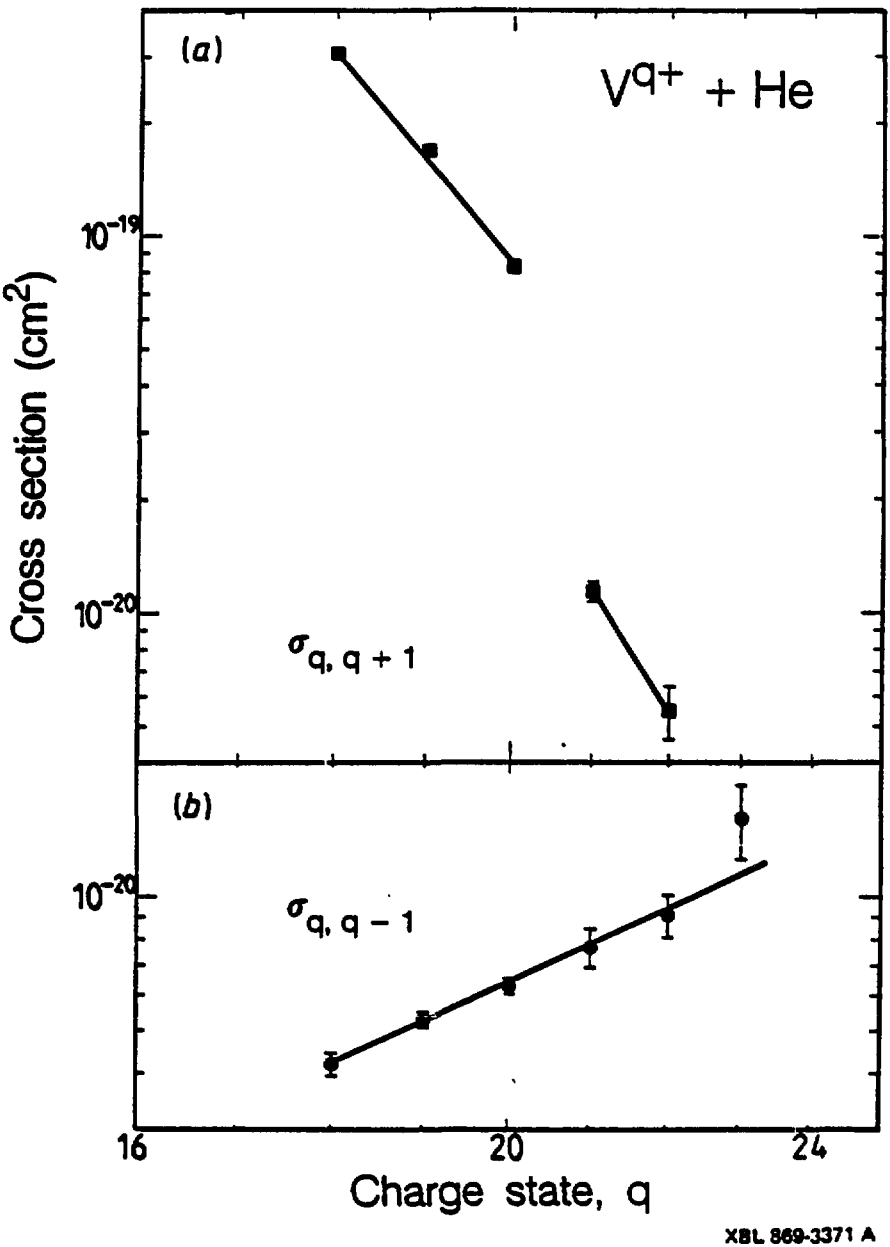
(a)
V^{q+} + He
10^{-19}
10^{-20}
Cross section (cm^2)
$\sigma_{q, q+1}$
(b)
10^{-20}
$\sigma_{q, q-1}$
16
20
24
Charge state, q
XBL 869-3371 A

Figure 2.

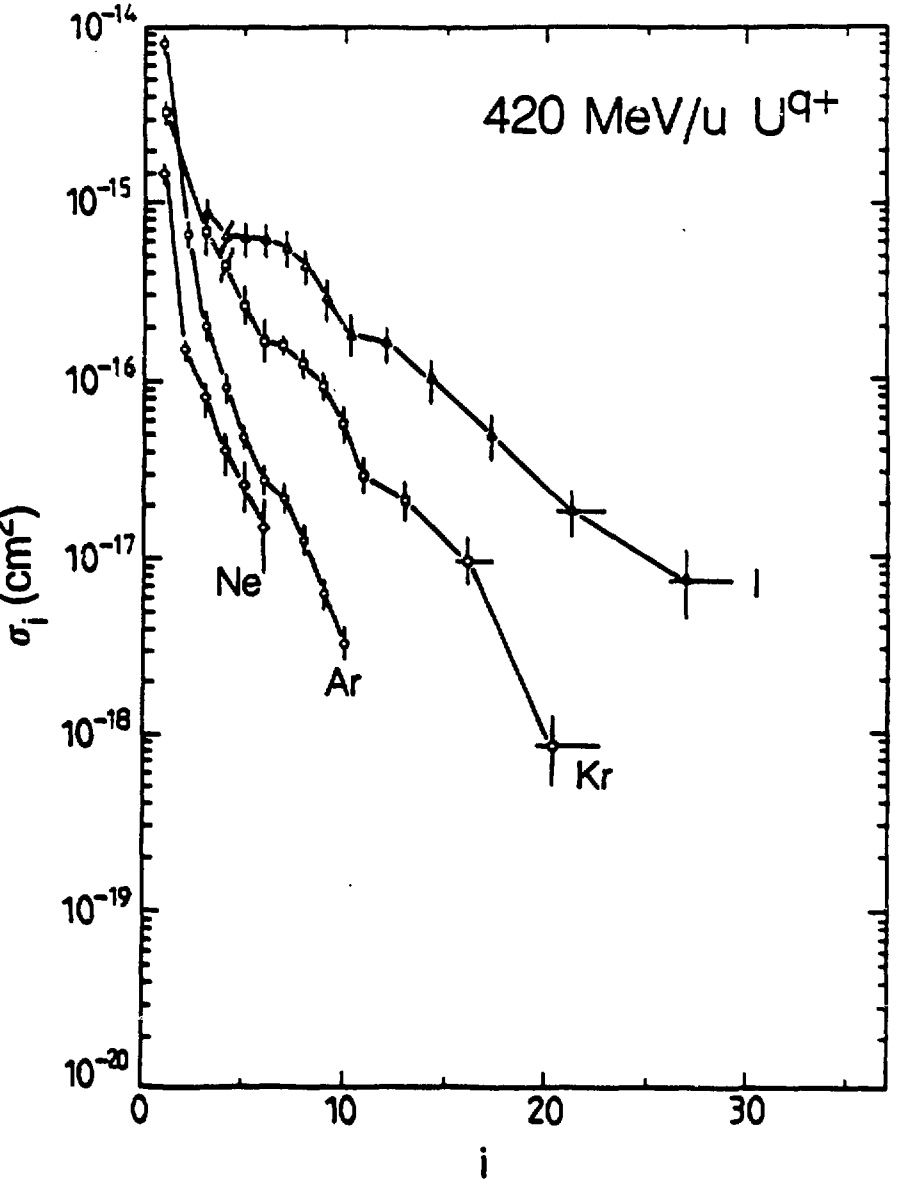

XBL 869-3369 A

Figure 3.

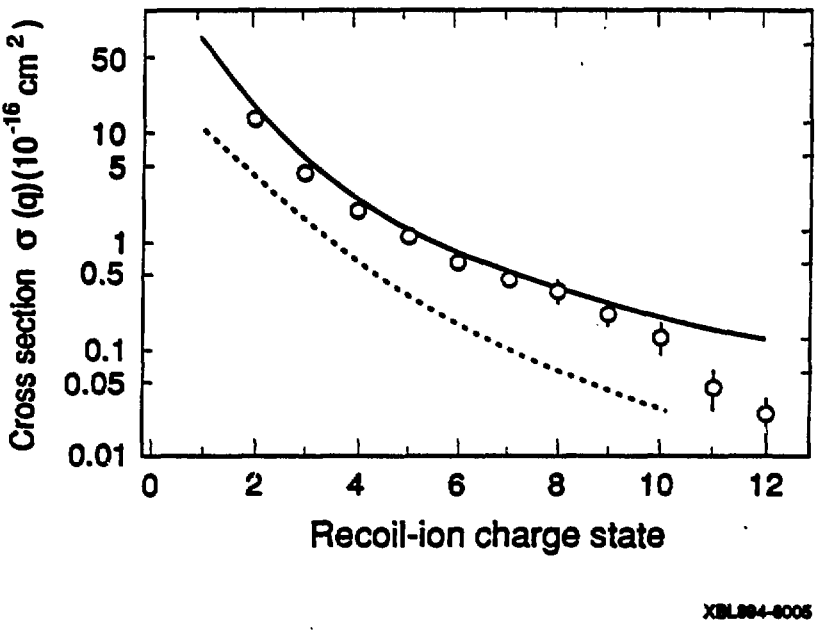
Cross section σ (q)(10^-16 cm^2)
50
10
5
1
0.5
0.1
0.05
0.01
0
2
4
6
8
10
12
Recoil-ion charge state
XBL894-6005

Figure 4.

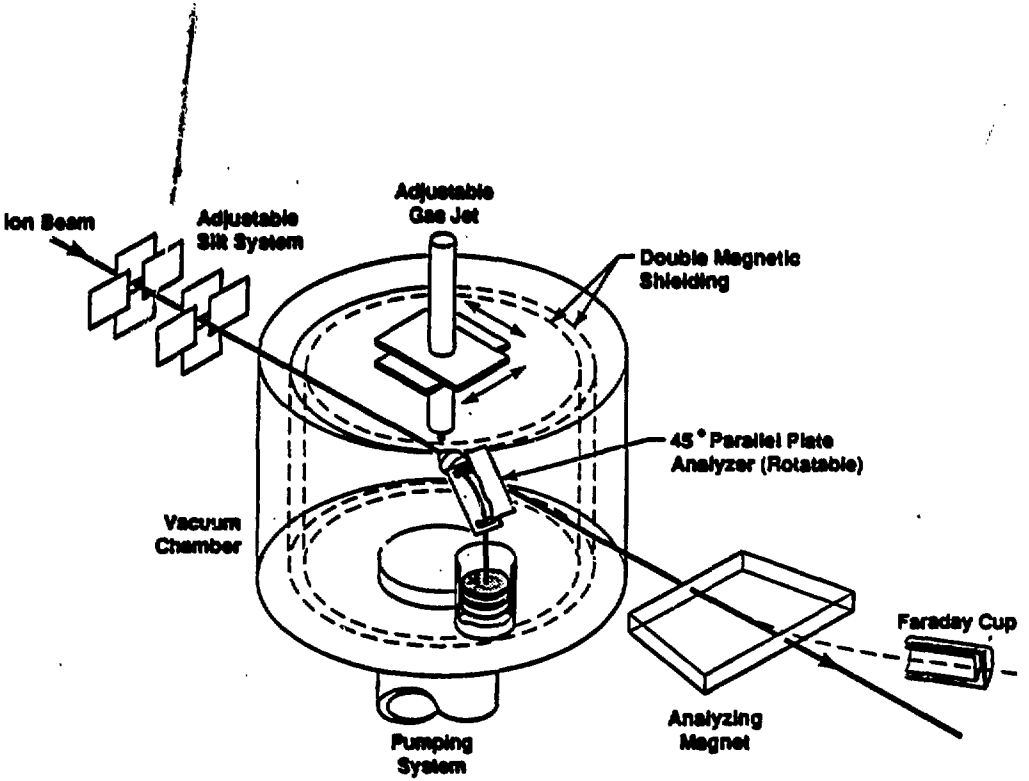
Ion Beam
Adjustable Slit System
Adjustable Gas Jet
Double Magnetic Shielding
45° Parallel Plate Analyzer (Rotatable)
Vacuum Chamber
Faraday Cup
Analyzing Magnet
Pumping System

Figure 5.

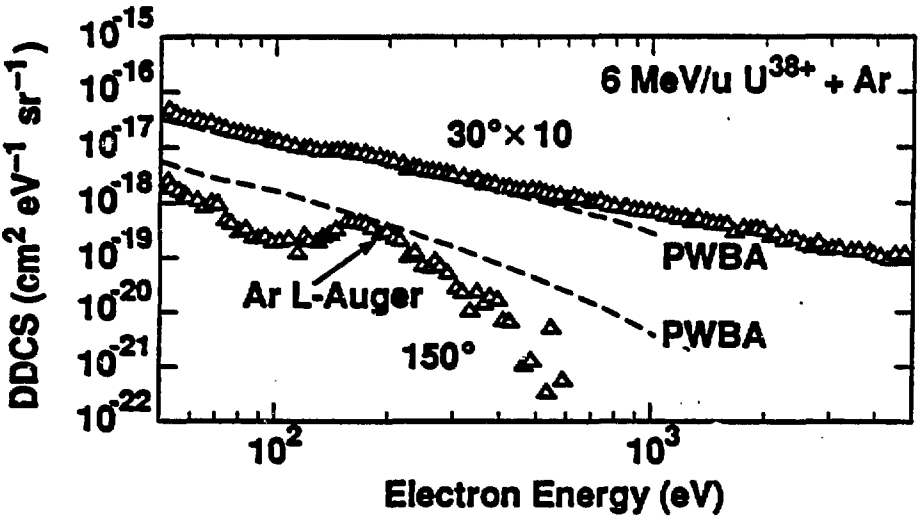
DDCS (cm^2 eV^{-1} sr^{-1})
10^{-15}
10^{-16}
10^{-17}
10^{-18}
10^{-19}
10^{-20}
10^{-21}
10^{-22}
6 MeV/u U^{38+} + Ar
30°×10
PWBA
Ar L-Auger
PWBA
150°
10^2
10^3
Electron Energy (eV)

Figure 6.

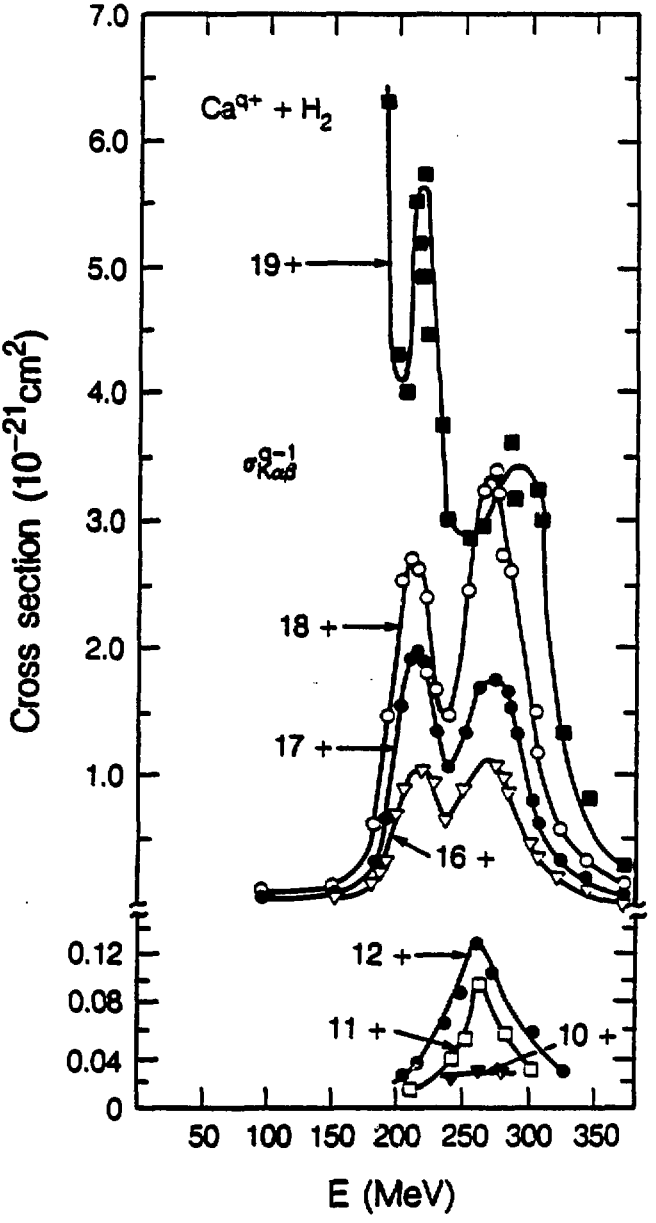
7.0
6.0
5.0
4.0
3.0
2.0
1.0
0.12
0.08
0.04
0
Cross section (10^{-21}cm^2)
$Ca^{q+} + H_2$
19+
18 +
17 +
16 +
12 +
11 +
10 +
$\sigma^{q-1}_{Ka\beta}$
50 100 150 200 250 300 350
E (MeV)
XBL 873-10029

Figure 7.

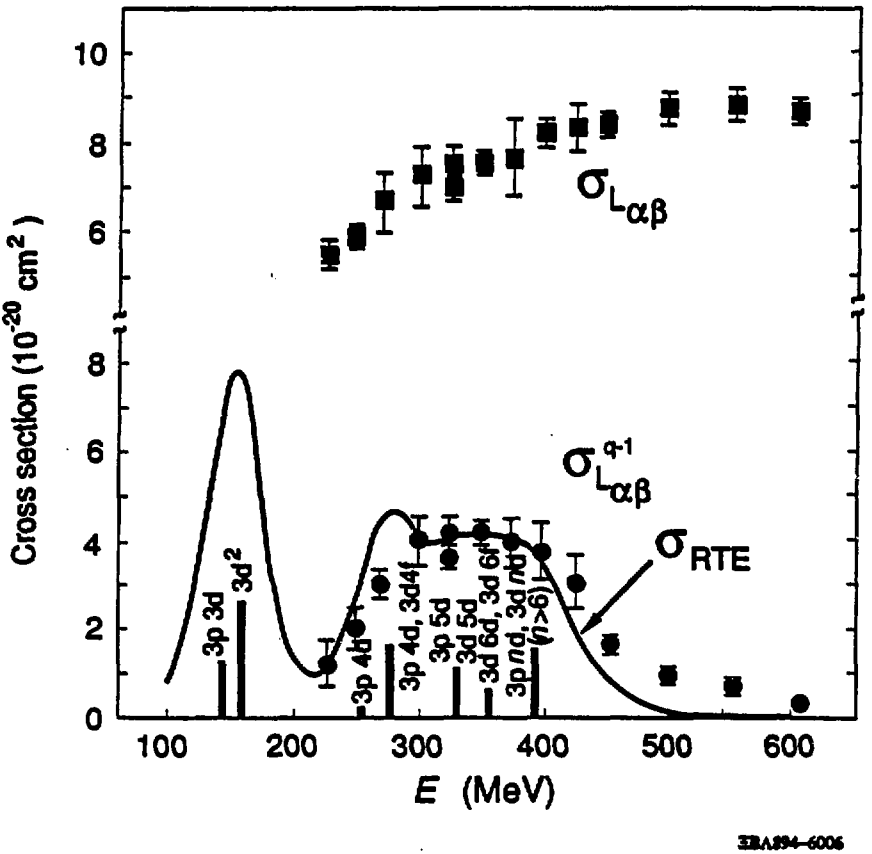
Cross section (10^{-20} cm^2)
E (MeV)
$\sigma_{L\alpha\beta}$
$\sigma^{q-1}_{L\alpha\beta}$
σ_{RTE}
3p 3d
3d^2
3p 4d
3p 4d, 3d4f
3p 5d
3d 5d
3d 6d, 3d 6f
3p nd, 3d nf (n>6)
3BA894-6006

Figure 8.

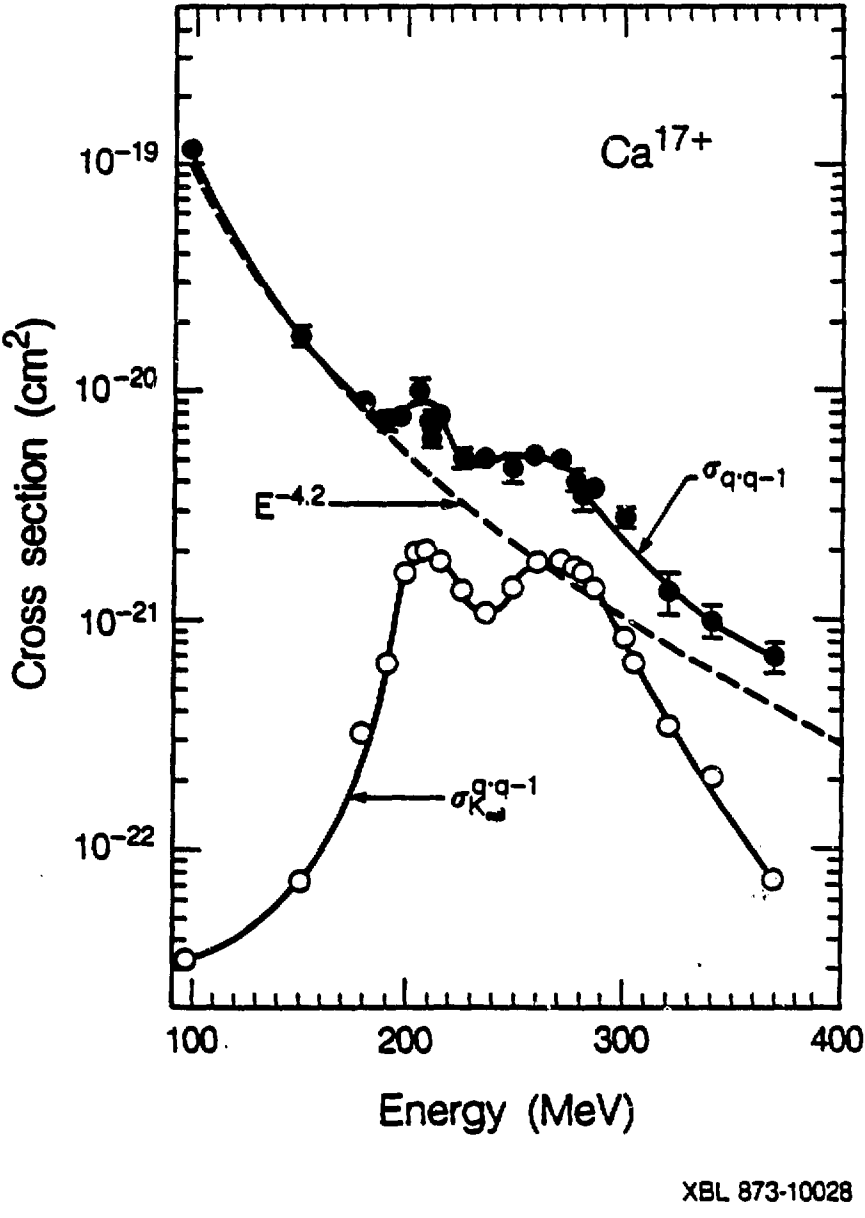
Ca17+
10-19
10-20
10-21
10-22
Cross section (cm2)
E-4.2
σq·q-1
σKq·q-1
100
200
300
400
Energy (MeV)
XBL 873-10028

Figure 9.

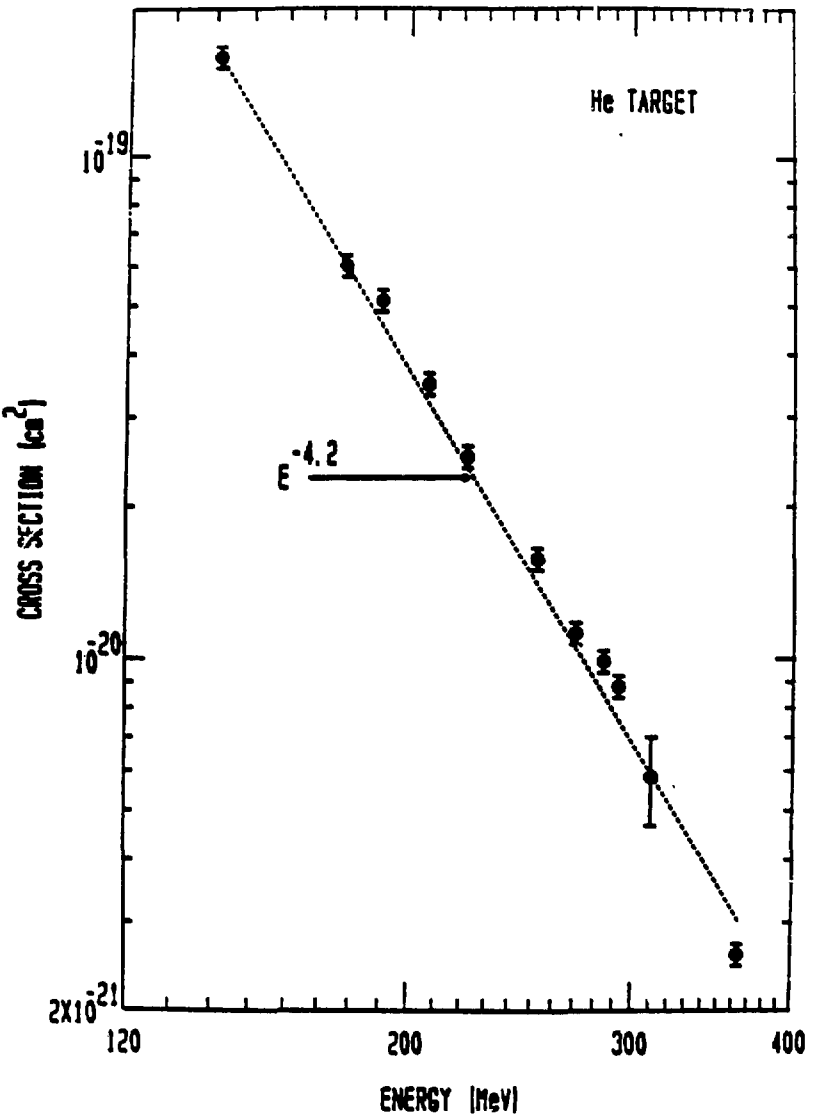
He TARGET
10^{-19}
10^{-20}
$2X10^{-21}$
CROSS SECTION (cm^2)
$E^{-4.2}$
120
200
300
400
ENERGY (MeV)
XBL 869-3372

Figure 10.

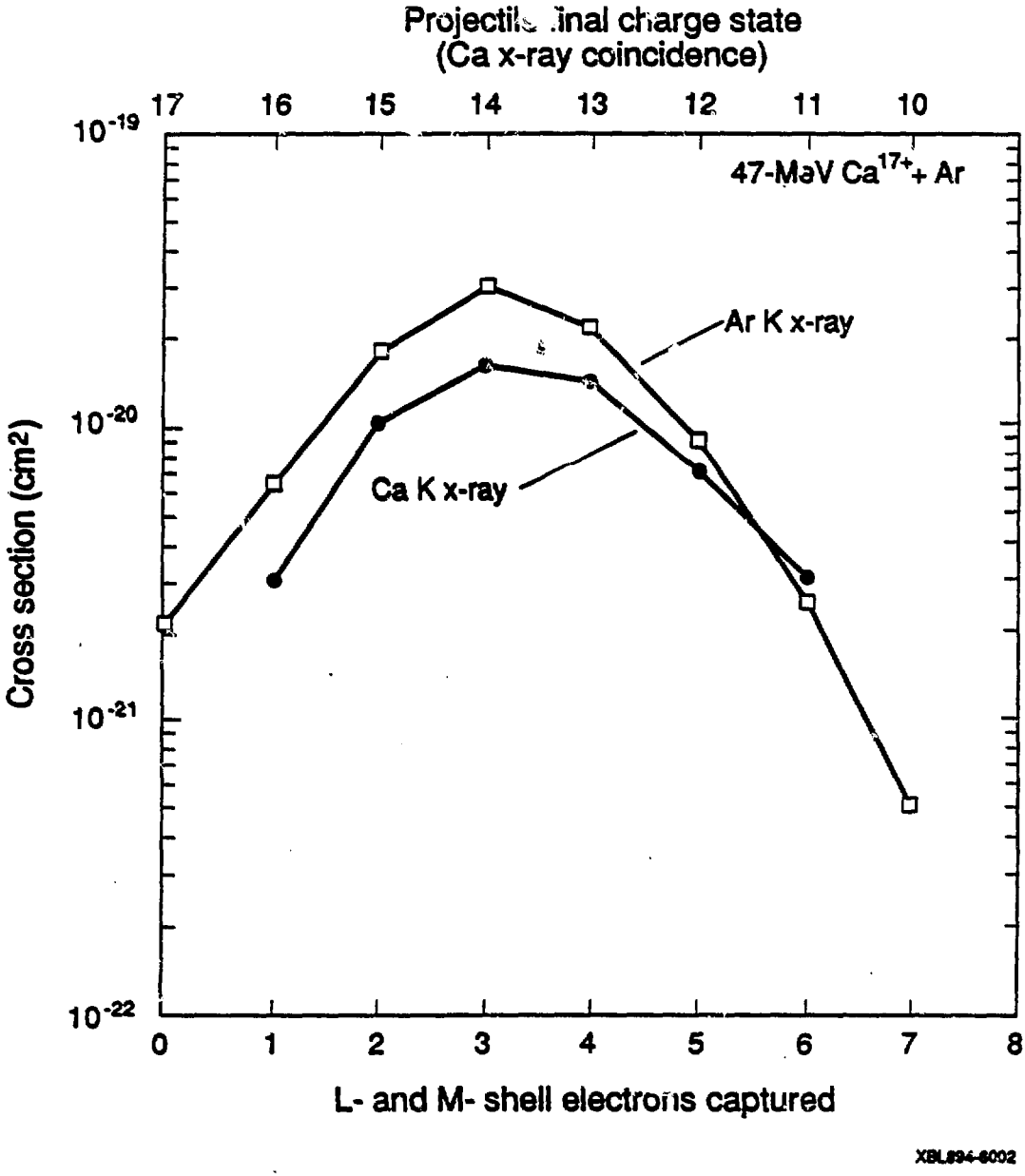
Projectile final charge state
(Ca x-ray coincidence)
17
16
15
14
13
12
11
10
47-MeV Ca17+ + Ar
Ar K x-ray
Ca K x-ray
Cross section (cm2)
10-19
10-20
10-21
10-22
0
1
2
3
4
5
6
7
8
L- and M- shell electrons captured
XBL894-6002

Figure 11.

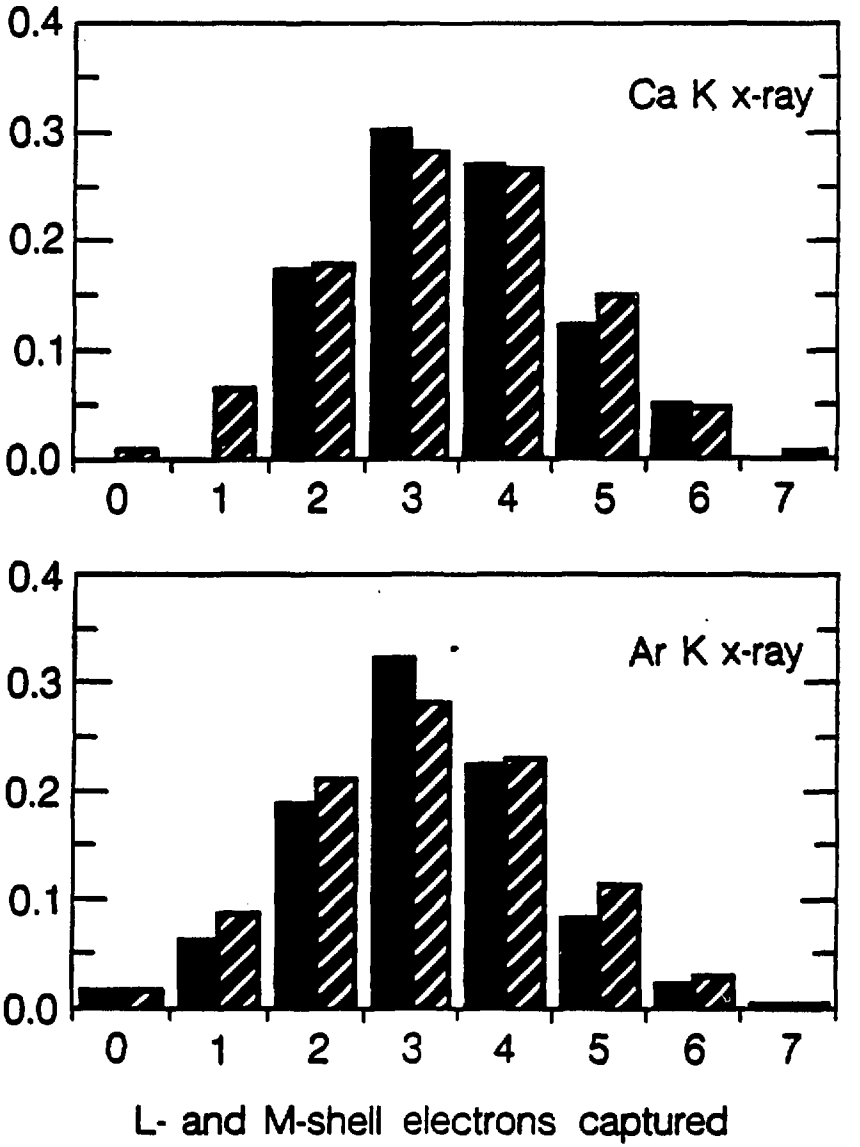
0.4
0.3
0.2
0.1
0.0
Ca K x-ray
0 1 2 3 4 5 6 7
0.4
0.3
0.2
0.1
0.0
Ar K x-ray
0 1 2 3 4 5 6 7
L- and M-shell electrons captured
XBL 8810-8577

Figure 12.

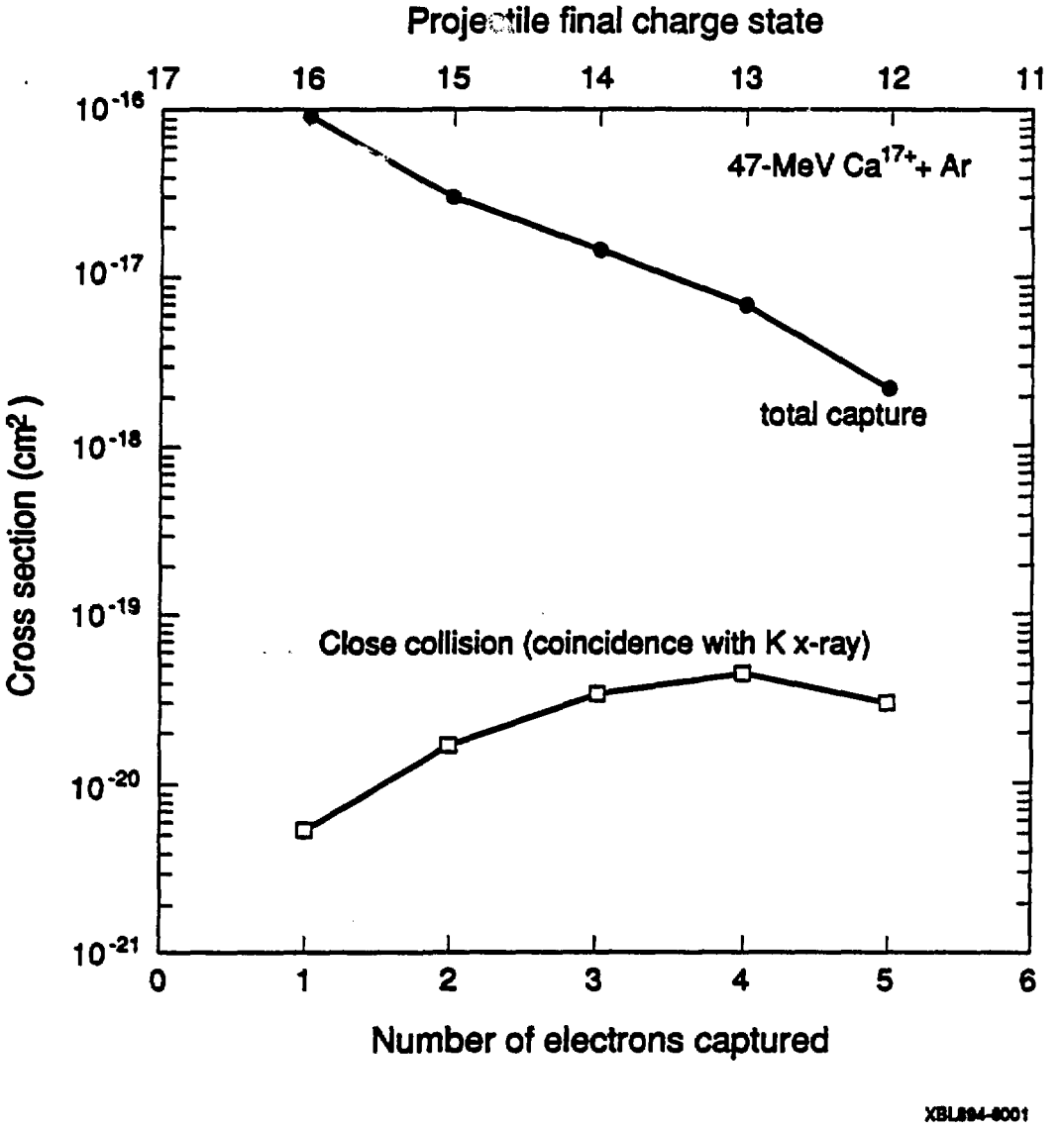
Projectile final charge state
17
16
15
14
13
12
11
10^{-16}
10^{-17}
10^{-18}
10^{-19}
10^{-20}
10^{-21}
47-MeV Ca^{17+} + Ar
total capture
Close collision (coincidence with K x-ray)
Cross section (cm^2)
0
1
2
3
4
5
6
Number of electrons captured
XBL894-6001

Figure 13.

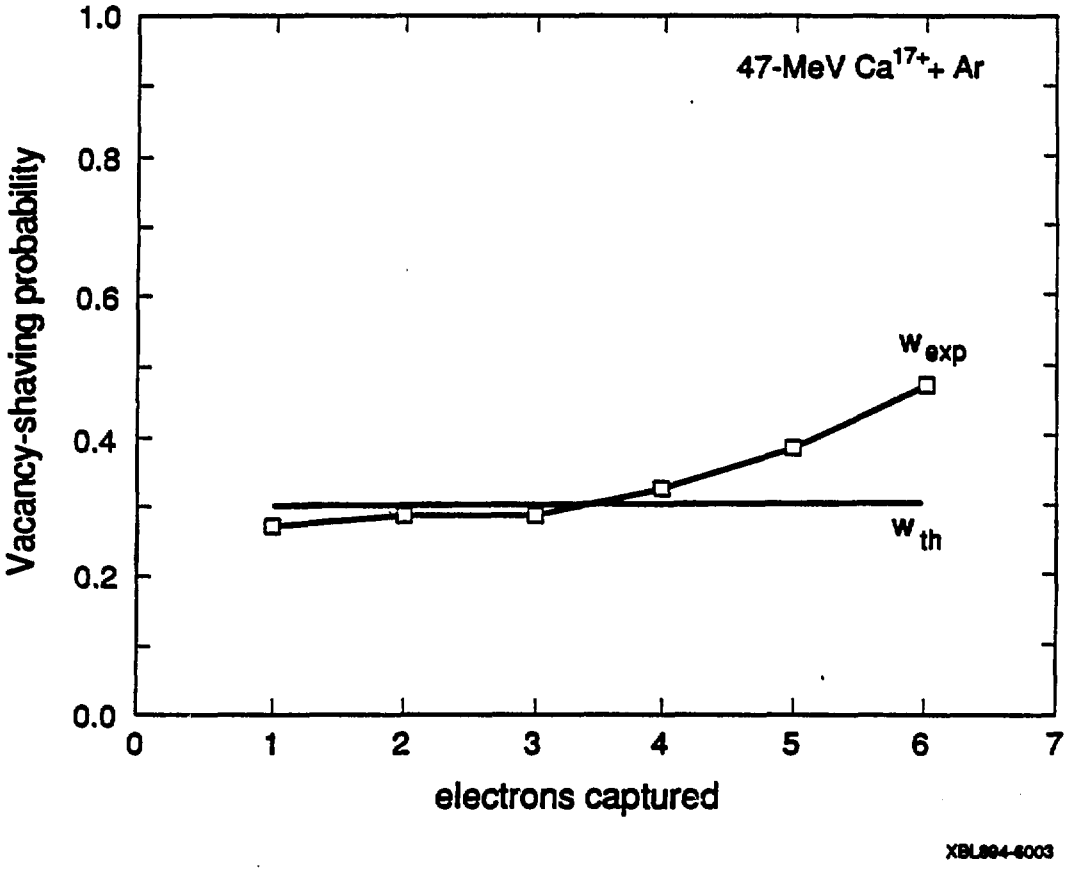
47-MeV Ca17+ + Ar
Wexp
Wth
Vacancy-shaving probability
electrons captured
1.0
0.8
0.6
0.4
0.2
0.0
0
1
2
3
4
5
6
7
XBL894-6003

Figure 14.

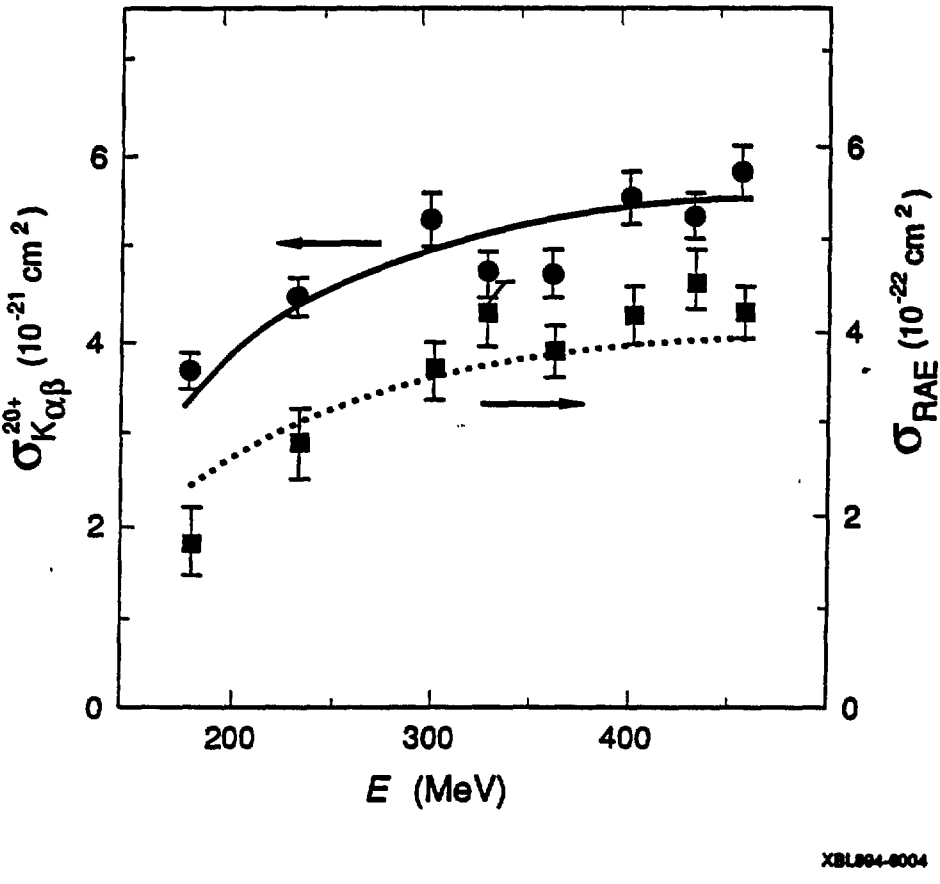
6
4
2
0
200
300
400
E (MeV)
$\sigma^{20+}_{K\alpha\beta}$ (10^{-21} cm^2)
σ_{RAE} (10^{-22} cm^2)
XBL894-6004

Figure 15.